ISPRS Journal of Photogrammetry and Remote Sensing 149 (2019) 146–156

Contents lists available at ScienceDirect

ISPRS Journal of Photogrammetry and Remote Sensing

journal homepage: www.elsevier.com/locate/isprsjprs

Integrating UAV optical imagery and LiDAR data for assessing the spatial relationship between mangrove and inundation across a subtropical estuarine wetland

Xudong Zhu[a,*], Yuwen Hou[a], Qihao Weng[a,b], Luzhen Chen[a]

[a] Key Laboratory of the Coastal and Wetland Ecosystems (Ministry of Education), Coastal and Ocean Management Institute, College of the Environment and Ecology, Xiamen, Fujian 361102, China

[b] Center for Urban and Environmental Change, Department of Earth and Environmental Systems, Indiana State University, Terre Haute, IN 47809, USA

ARTICLE INFO

Keywords:
UAV
LiDAR
Mangrove
Zonation
Inundation
Zhangjiang Estuary

ABSTRACT

Mangrove-inundation patterns have been examined in many field studies, but spatially explicit quantitative analyses are still lacked. A better understanding of how mangrove species responds to the inundation gradient will facilitate mangrove conservation and management. In this study, we integrated unmanned aerial vehicle (UAV) camera imagery and light detection and ranging (LiDAR) data for exploring mangrove-inundation spatial patterns over the intertidal zone in a subtropical estuarine wetland (Zhangjiang estuarine wetland, Fujian, China). Our results indicated that > 90% of mangrove forests (mainly *Kandelia obovate*, *Avicennia marina*, and *Aegiceras corniculatum*) were situated within a one-meter elevation range between local mean sea level and higher high water, and the spatial distribution of mangrove forests showed hump-shaped patterns along the inundation gradient with favorable inundation periods of 2 ~ 5 h per day. Our analyses further indicated that there was a weak mangrove zonation pattern with overlaps between species zones along the elevation gradient, and that mangrove species had differential inundation sensitivities with *Avicennia marina* being most sensitive to the inundation stress. To the best of our knowledge, this is the first spatially explicit quantitative study to examine the influences of inundation regime on both spatial distribution and canopy height of different mangrove species over the intertidal zone at the landscape scale. This study highlights the practicability and necessity of UAV LiDAR in interpreting mangrove-inundation spatial patterns, and confirms the importance of inundation regime as a key driver in regulating the spatial patterns of mangrove forests. The determination of appropriate elevation ranges and inundation periods provides some important knowledge to guide mangrove restoration practices and to assess the vulnerability of mangrove forests in response to future sea level rise.

1. Introduction

Mangrove forests, one of the most important coastal blue carbon ecosystems, are distributed within limited intertidal zone typically between mean seal level (MSL) to highest spring tide in coastal tropical and subtropical climates in the world (Alongi 2009; Giri et al. 2010). Mangrove forests provide critical ecosystem services such as protection from erosions, carbon sequestration, maintaining biodiversity (Costanza et al. 1997; Donato et al. 2011; Alongi 2014). However, mangrove forests are now threatened globally with significant loss in area and severe degradation in habitats mainly due to human activities including land conversion to aquaculture, agriculture, urban development (Valiela et al. 2001; Giri et al. 2010). Future climate change, sea level rise and more intensive human activities will much likely make it worse for mangrove forests. Therefore, sound conservation and management practices of mangrove forests are highly needed. To achieve this, the first step is to enhance our limited understanding of mangrove ecology including the key factors influencing the distribution and growth of mangrove species.

The distribution of mangrove species in the intertidal zone is subjected to multiple environmental gradients (inundation, salinity, soil texture, nutrients, etc.) and the spatial interactions of these gradients are complex and site-dependent (Krauss et al. 2008). Among these proposed environmental drivers, tidal inundation regime (i.e., flooding frequency and duration) has been widely reported as a key driver governing mangrove species distribution (Chen et al. 2013; Crase et al. 2013; Spier et al. 2016; Leong et al. 2018), since tidal activities are relatively easy to be documented and are closely linked to other drivers

* Corresponding author at: College of the Environment and Ecology, Xiamen University, Xiamen, Fujian 361102, China.
E-mail address: xdzhu@xmu.edu.cn (X. Zhu).

https://doi.org/10.1016/j.isprsjprs.2019.01.021
Received 19 September 2018; Received in revised form 21 January 2019; Accepted 22 January 2019

including salinity, soil texture, and redox potential. Indeed, the link between tidal inundation and species distribution has been widely discussed in mangrove ecology for nearly a century, asserting that coastal mangrove forests exhibit zonation of species along the elevation gradient (Watson 1928; Chapman 1976; Snedaker 1982). The relationships between tidal inundation regime and mangrove species distribution are appealing to mangrove ecologists in three aspects: (1) to understand underlying mechanisms of mangrove forests adapting to flooding intertidal zone (Naidoo 1983; Chen and Wang 2016), (2) to support mangrove restoration practices by indicating appropriate elevation ranges for different mangrove species (Kodikara et al. 2017; Oh et al. 2017), and (3) to assess the vulnerability and resilience of mangrove forests to future sea level rise (Nitto et al. 2014; Lovelock et al. 2015). There are already a number of laboratory and field studies exploring the inundation-mangrove relationships, but the influence of inundation regime on mangrove forests is still poorly understood and quantitative mangrove-inundation relationships have not been well documented (Krauss et al. 2006).

To analyze mangrove-inundation relationships in a quantitative manner, it is essential to accurately measure the spatial variability of tidal inundation regime; however, this is challenging in the intertidal zone vegetated with mangrove forests which have a flat landscape but complex microtopography (e.g., small creeks and basins). The characterization of microtopography is important since the distribution and growth of mangrove species are affected by small differences in elevation (Oh et al. 2017). Tidal gauge measurements can capture the temporal dynamics of tidal inundation regime at single-point scales, but they are not able to characterize the spatial variability of tidal inundation regime across the intertidal zone. In many of field studies exploring the inundation-mangrove relationships, single-point measurements of tidal water level and ground-based spatial surveying of surface elevation with high-accuracy instruments (such as real-time kinematic GPS) are often combined to estimate the spatial variability of inundation regime (Ellison et al. 2000; Crase et al. 2013; Leong et al. 2018), assuming that intertidal zone of equal surface elevation have the same inundation regime. The ground-based surface elevation surveying is time-consuming and labor-intensive due to the inaccessibility of many mangrove forests. It might be suitable for those studies only focusing on several mangrove transects (e.g., Ellison et al. 2000); however, it is much challenging to apply this method to characterize the spatial variability of surface elevation across the intertidal zone with complex microtopography particularly under dense mangrove canopies.

Many remote sensing data, such as SRTM, ICESat/GLAS, TanDEM-X, and ALOS PALSAR, from spaceborne interferometric synthetic aperture radar (InSAR) and light detection and ranging (LiDAR) instruments have been used to characterize large-scale spatial variability of terrain and vegetation information in coastal wetlands (Cornforth et al. 2013; Fatoyinbo and Simard 2013; Kovacs et al. 2013; Lee and Fatoyinbo 2017). As examples, Fatoyinbo and Simard (2013) estimated canopy heights of all mangroves in Africa at continental scale from SRTM and ICESat/GLAS data, and Lee and Fatoyinbo (2017) developed inversion approaches using TanDEM-X data to estimate mangrove canopy heights showing the possibility of global-scale applications. These remote sensing data from spaceborne instruments have shown great potentials for generating large-scale canopy height model (CHM) of mangrove forests, but they have relatively low spatial resolutions (tens of meters) and height accuracy (error in meters) (Lucas et al. 2017), which restricts them from local-scale studies. At local scales, stereo photogrammetry using very high resolution (VHR) images from unmanned airborne vehicle (UAV) and satellites has been used to generate CHM of mangrove forests (e.g., Lucas et al. 2002), but this method still suffers from low accuracy (error in meters) in estimated mangrove canopy heights.

With the developments of UAV and LiDAR technologies and the reduce in the expense of applying these technologies, UAV LiDAR remote sensing has been increasingly used to characterize coastal terrains and vegetation structures (Morris et al. 2005; Lagomasino et al. 2016; Fatoyinbo et al. 2017; Wannasiri et al. 2013). On the one hand, the ability of UAV LiDAR to measure surface elevation with high accuracy even under dense forest canopies makes it ideal to detect the spatial variability of microtopography over the intertidal zone (Crase et al. 2013), which is then combined with tidal water level measurements to map the spatial distribution of inundation regime. On the other hand, the ability to acquire forest canopy heights at a centimeter accuracy level from LiDAR-derived CHM (Feliciano et al. 2017) provides an ideal opportunity to examine the influences of inundation regime on the growth of mangrove species at the landscape scale. Although airborne LiDAR has been often proposed as the most accurate way for forest structure measurements in various forest types (Zhao et al. 2012; Zolkos et al. 2013; Duncanson et al. 2015), only a few airborne LiDAR applications have been done so far for mangrove forests and the practicability of these applications has not been well verified.

In this study, we integrate UAV camera and LiDAR data for exploring mangrove-inundation spatial patterns across a subtropical estuarine wetland. The main goal of this study is to quantitatively evaluate the role of inundation regime in governing the spatial distribution and growth of different mangrove species at the landscape scale. Our specific objectives are to examine (1) how different mangrove species occur along the gradients of elevation and inundation, and (2) how the mangrove-inundation spatial patterns differ among species.

2. Method and materials

2.1. Study area

The study area is a subtropical intertidal wetland with an area of $\sim$2.6 km^2, located to the south of Zhangjiang estuary in the southeast coast of China (Yunxiao, Fujian, China; Fig. 1a). This region has a mangrove area of $\sim$0.5 km^2 mainly including *Kandelia obovate* (*K. obovata*), *Avicennia marina* (*A. marina*), and *Aegiceras corniculatum* (*A. corniculatum*), as well as invasive *Spartina alterniflora* (*S. alterniflora*). The three main mangrove species have distinct color characteristics in early summer ([1]dark-green for *K. obovata*, grey for *A. marina*, and yellow-green for *A. corniculatum*; Fig. 1b-d). The wetland has a monsoon climate with annually mean rainfall of 1714.5 mm mostly occurring from April to September, and has annually mean air temperature of 21.2 °C and relative humidity of 79% (Lin 2001). The wetland experiences an irregular semidiurnal tide with annually mean tide range of 2.3 m and varying tidal water salinity up to 15 PSU. All necessary permits on in-situ research activities in this study were acquired from the Zhangjiang Estuary Mangrove National Nature Reserve Administration, and more details on biotic and abiotic resources of the reserve can be found in Lin (2001).

2.2. UAV LiDAR data acquisition and processing

The LiDAR raw data were collected by RedChina Geosystems, Inc., using UAV-borne (model: DJI M600) HawkScan HS-600 scanning system within low-tide time windows during Oct. 23-25th, 2017. The UAV flew at a height of $\sim$100 m, and the scanning system, comprised of a LiDAR scanner (RIEGL VUX-1UAV with 0.5-cm relative and 1-cm absolute ranging accuracies) and a GNSS-Inertial positioning/navigation sensor (Trimble APPLANIX APX-15 with 2-cm horizontal and 5-cm vertical positioning accuracies), had horizontal and vertical positioning accuracies of 7 $\sim$ 8 cm and 5 $\sim$ 10 cm, respectively. The raw data were processed to produce LiDAR point cloud with a density of $\sim$100 points/m^2, which was dense enough to have points penetrate dense mangrove canopy and reach bare surface. The classification of point cloud into

[1] For interpretation of color in Fig. 1, the reader is referred to the web version of this article.

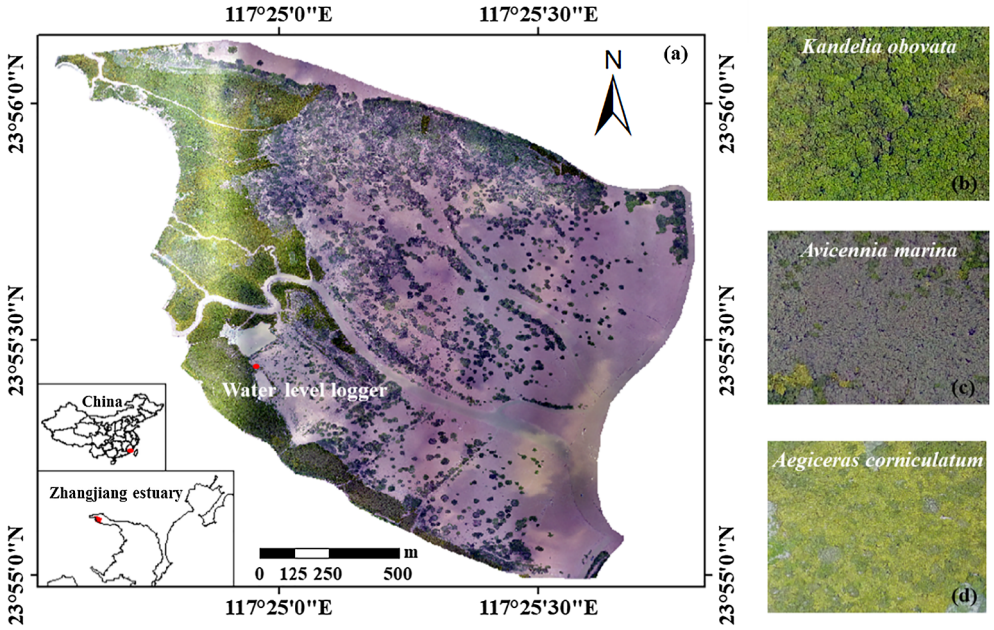

Fig. 1. The overview landscape and geolocation of Zhangjiang estuarine wetland (a) with typical images of three main mangrove species: (b) *Kandelia obovata*, (c) *Avicennia marina*, and (d) *Aegiceras corniculatum*. The images were acquired from UAV on Jun. 29th, 2017.

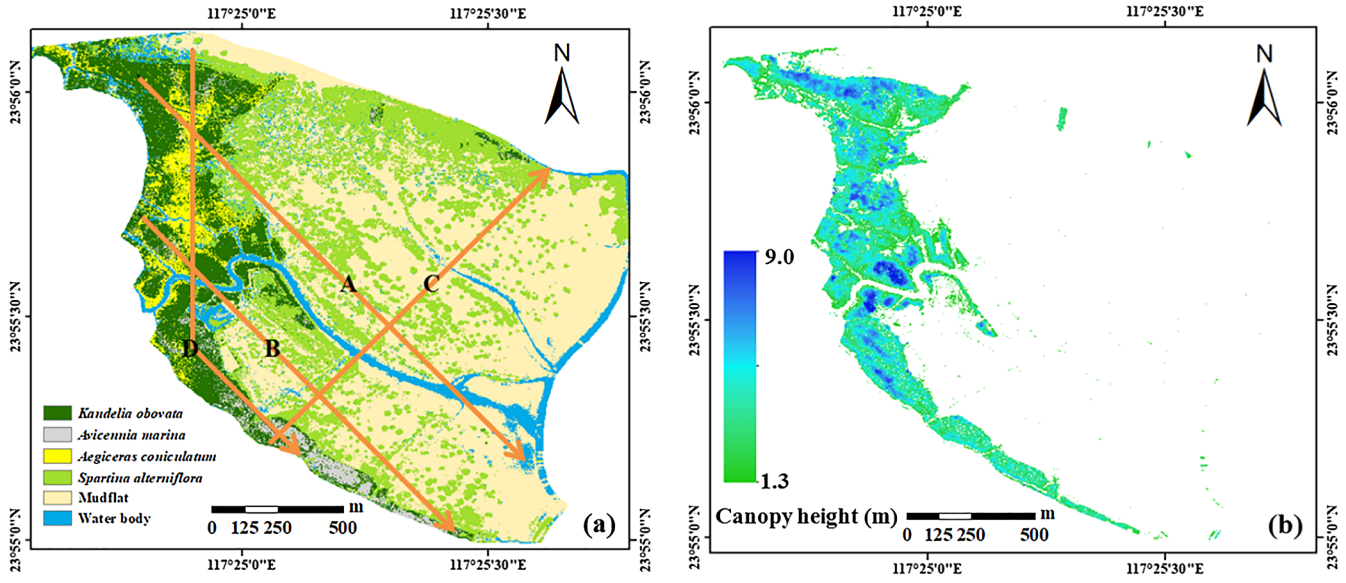

Fig. 2. Spatial distribution of (a) different land cover types including three main mangrove species and (b) mangrove canopy height in meters over Zhangjiang estuarine wetland, derived from UAV camera and LiDAR data. Arrows over the wetland indicate the four selected transects used in Fig. 4.

vegetation points and ground points was performed in TerraScan software (Terrasolid Limited, Helsinki, Finland) according to the geometric characteristics of the point cloud (Axelsson 2000; Soininen 2012). The classified points were further processed to produce digital surface model (DSM) and digital elevation model (DEM) with a spatial resolution of 1 m. Canopy height model (CHM) was then calculated as the difference between DSM and DEM.

2.3. UAV imagery collection and processing

For mapping mangrove species, an orthomosaic image with the same spatial resolution (1 m) as LiDAR data products was generated from a set of UAV camera images after a procedure of image acquisition and processing. First, we conducted several UAV flights (UAV platform: DJI Phantom 4; RGB camera: 1″ CMOS with 12 M pixels; flight height: ~200 m; flight speed: ~10 m/s) around noon on Jun. 29th, 2017, at low-tide conditions, to collect a set of camera images (~500) over the wetland. All UAV flights were finished within a short time window (< 2 h) to avoid large variation in light conditions, and enough image overlaps for image processing (> 80% forward overlap and > 60% side overlap) were considered during the flights.

Second, using multi-view 3D reconstruction technology, camera images were processed in Photoscan software (Agisoft LLC, St. Petersburg, Russia) to generate a VHR orthomosaic image (spatial resolution of ~0.08 m) covering the whole wetland. The spatial resolution of the orthomosaic image was reduced to the same resolution (1 m) as LiDAR data products, and then the image was then geographically registered with LiDAR data products (image-to-image registration with root mean square error < 0.5 m) using a set of clear control points based on visual identification from the images (~20 points distributed

Table 1
Accuracy assessment of the land cover classification of UAV imagery (KO - *Kandelia obovate*, AM – *Avicennia marina*, AC – *Aegiceras coniculatum*, SA – *Spartina alterniflora*, MF – mudflat, WB – water body) based on the validation sample set. The area of each class was expressed as percentage of total area of all classes in the validation sample set. Producer's and user's accuracy were calculated for each class and all mangrove species (mean values in italic). Overall classification accuracy for all classes was summarized from the values on the diagonal (in italic).

		Area of each class (% of total area of all classes)						User's accuracy (%)	
		KO (2.6)	AM (3.1)	AC (4.0)	SA (25.2)	MF (41.7)	WB (23.4)		
Classified area of each class (% of total area of all classes)	*KO*	*2.5*	0.6	0.8	0.0	0.0	0.0	64.4	
	AM	0.0	*2.4*	0.0	0.0	0.0	0.0	99.6	*Mean:* ***86.9***
	AC	0.1	0.0	*3.0*	0.0	0.0	0.0	96.8	
	SA	0.0	0.1	0.0	*20.7*	0.3	0.1	97.6	
	MF	0.0	0.0	0.0	4.2	*37.0*	10.4	71.8	
	WB	0.0	0.0	0.1	0.4	4.5	*13.0*	72.6	
Producer's accuracy (%)		97.3	77.4	76.0	81.9	88.7	55.4	*Overall accuracy:* ***78.6***	
		Mean: ***83.6***							

over the region).

Third, we applied maximum likelihood classification (MLC) to map the spatial distribution of mangrove species based on the combination of RGB information of the orthomosaic image and canopy height information of LiDAR-derived CHM data. The MLC is one of the most widely used supervised classification algorithms and it assigns each pixel of imagery to a particular class based on *a priori* calculated probabilities from the training samples (Liu et al. 2002). The MLC is a parametric classifier assuming the samples of each class follow normal distribution. Given that the orthomosaic image from our UAV flights had a very high spatial resolution (originally at ~0.08 m), we produced the reference sample set for each land cover class (i.e., *K. obovate*, *A. marina*, *A. coniculatum*, *S. alterniflora*, mudflat, and water body) based on expert knowledge in visual image interpretations and in-situ validations in multiple field surveys. The reference sample set (~30 thousand samples or m^2) was created by spatially random sampling and the number of samples for each class was roughly proportional to initial visual estimation of the area of each class. Four fifths of samples for each class in the reference sample set were used for training sample set of the MLC and the rest were reserved as the validation sample set for accuracy assessment including the producer's, user's, and overall accuracies.

2.4. Tidal measurements and spatial extrapolation

Single-point time series of tidal water levels were estimated from pressure measurements using HOBO U20L-04 Water Level Logger (Onset, Bourne, MA, USA) deployed just above sediment surface near the fringe of mangroves (Fig. 1a). The time series was recorded at a 10-min interval, and all 10-min measurements within a period of one year (Sep. 20th, 2016 ~ Sep. 20th, 2017) were used in this study to characterize annually mean tidal regime. Since the elevation of the water level sensor was not deployed low enough and the sensor only recorded valid measurements when inundated, we were not able to capture a complete water level curve. To overcome this issue, we used a gap-filling procedure to derive a complete one-year water level curve by fitting in-situ water level time series to tidal forecast table of nearby site (Dongshan site; ~20 km seawards) from State Oceanic Administration, China: (1) for a given tidal cycle (a lunar day; ~24.8 h), we compared incomplete time series (i.e., upper portion of tidal water level curve) to corresponding time series of water level at Dongshan site, and fit a regression line between these two time series; (2) the regression relationship was applied to estimate lower portion of tidal water level curve (not measured by in-situ Water Level Logger) to form a complete water level curve; (3) we repeated these two steps for all tidal cycles to derive a complete one-year water level curve.

Based on the complete one-year water level curve, we calculated MSL of the wetland as arithmetic mean of one-year water level time series, and then defined the elevation of MSL as zero (MSL had a relative elevation of zero). Once MSL was determined, LiDAR-derived DEM data was converted from absolute elevation to relative elevation (positive/negative values for pixels above/below MSL). The annually mean inundation period (indicated by 0 ~ 24 h per day) was calculated from the complete one-year water level curve for any relative elevation (approximate 12 h per day at relative elevation of zero), resulting in an inundation map showing the spatial distribution of annually mean inundation period (spatial resolution of 1 m). Following Pugh and Faull (1983), four critical values of relative elevation in addition to MSL were determined from mean water level curve over the one-year period, including higher high water (HHW), lower high water (LHW), higher low water (HLW), and lower low water (LLW). Based on these critical relative elevations, we defined six inundation areas according to different inundation regimes: fully exposed area (FEA; above HHW), partially exposed area (PEA; between HHW and LHW), above MSL area (AMA; between LHW and MSL), below MSL area (BMA; between MSL and HLW), partially inundated area (PIA; between HLW and LLW), fully inundated area (FIA; below LLW).

3. Results

3.1. Spatial distributions of mangrove species and inundation regime

Based on high-resolution spatial data of UAV camera and LiDAR CHM, the orthomosaic image was classified into different land covers

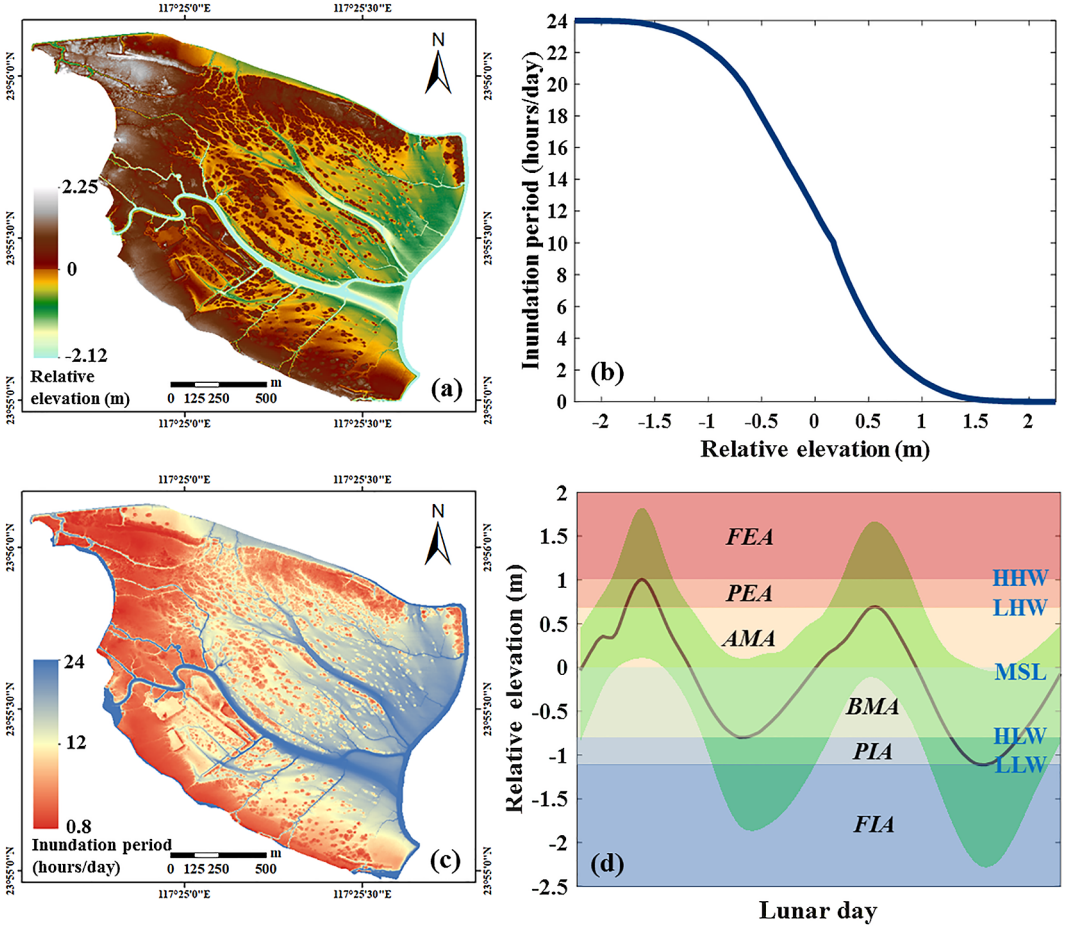

Fig. 3. Spatial distributions of (a) relative elevation (meter) and (c) annually mean inundation period (hours per day) over Zhangjiang estuarine wetland. The quantitative relationship between relative elevation and inundation period over this wetland was illustrated (b). Mean water level curve over a lunar day (solid line) with varying ranges (shaded area), derived from one-year tidal measurements, was shown for characterizing tidal inundation regime (d). Five relative elevations and corresponding six inundation areas were marked for higher high water (HHW), lower high water (LHW), mean sea level (MSL), higher low water (HLW), lower low water (LLW), fully exposed area (FEA), partially exposed area (PEA), above MSL area (AMA), below MSL area (BMA), partially inundated area (PIA), fully inundated area (FIA).

including three main mangrove species, *S. alterniflora*, mudflat, and tidal creeks (Fig. 2a). The land cover map had an overall classification accuracy of 78.6% across different land covers and mean producer's and user's accuracy of 83.6% and 86.9% respectively for mangrove species (Table 1). Almost all mangrove forests over Zhangjiang estuarine wetland were situated in the west of the intertidal zone with woody canopies, which made them easily discerned from other non-vegetated areas or vegetated area with herbaceous *S. alterniflora*. *K. obovate* (67.48% in areal proportion) was more widely distributed in space over the region of mangrove forests compared to the other two species. *A. marina* (12.12% in areal proportion) was mainly situated in the southern part of mangrove forests, while *A. corniculatum* (20.4% in areal proportion) was more distributed on the north of the main tidal creek meandering across the wetland. Mangrove forests over this wetland had canopy heights ranging from 1.3 to 9.0 m (mean height of 3.1 m, medium height of 4.5 m) and the tallest forest canopies were situated near the main tidal creek (Fig. 2b).

The characteristics of semidiurnal tide in Zhangjiang estuarine wetland were obviously revealed from the one-year tidal water level measurements with a mean tide range of 2.1 m (Fig. 3d). During this one-year period, tidal water levels had periodical but irregular temporal variations reaching up to 1.8 m above MSL and low to 2.2 below MSL. The relative elevations of four critical water levels were estimated to be 0.98 m, 0.77 m, −0.80 m, and −1.21 m for HHW, LHW, HLW, and LLW, respectively. Although only one-year period of tidal water levels was used to characterize the tidal inundation condition of Zhangjiang estuarine wetland, this one-year period of tidal data can be used to represent long-term tidal condition, given that monthly tidal data (mean high water, mean low water, and mean tidal range) within this one-year period is very close (within a difference of 20 cm in tidal water level) to long-term tidal conditions over the past two decades at nearby Dongshan tidal station (data not shown). The map of relative elevation over Zhangjiang estuarine wetland indicated a northwest-southeast trend with an elevation range of 4.4 m decreasing from 2.3 m to −2.1 m (Fig. 3a). The northwestern part of the wetland vegetated with mangrove forests had the highest relative elevation, while the eastern part of the wetland with several tidal creeks had the lowest relative elevation. Corresponding to the spatial pattern of relative elevation, the distributions of inundation period were mapped using the inundation-elevation curve (Fig. 3b), which had a declining gradient of ~1 h/decimeter within the mean tide range (~1 m below and above MSL). Same to relative elevation, the inundation period over this wetland showed a northwest-southeast trend increasing from several hours in mangrove forests to 24 h per day in tidal creeks (Fig. 3c). Note that there were many artificial "islands" in those area vegetated with *S. alterniflora*, since relative elevation might have been overestimated due to the fact that UAV LiDAR had poor ability to penetrate dense *S. alterniflora* canopy.

To further illustrate the changes in land covers across the wetland, four transects were selected to explore the distribution of land covers

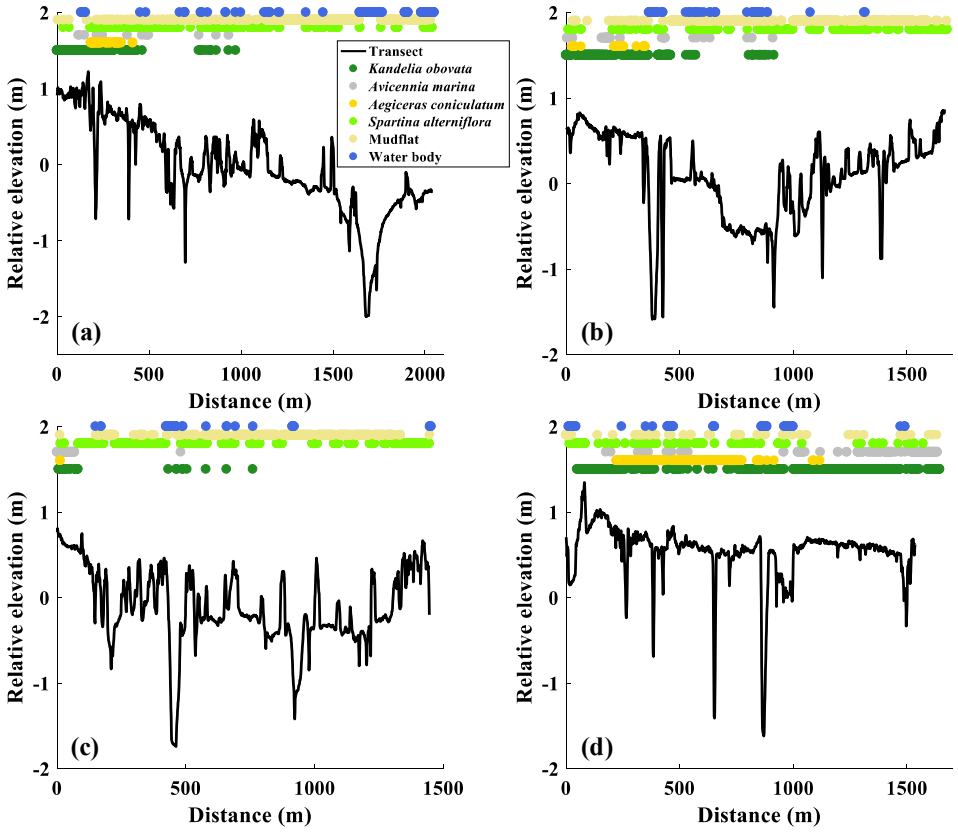

Fig. 4. Changing relative elevation and land cover types along four transects across Zhangjiang estuarine wetland (a-d correspond to transect A-D, respectively, as shown in Fig. 2a).

along the gradients of relative elevation and inundation period (Figs. 2 and 4). Among four transects, transect A trending from northwest to southeast had the steepest elevation slope (~0.1%) with a 2-m elevation change within a 2-km distance from the shoreline, while transect D trending from north to south and to southeast had the slowest elevation slope. The fluctuant elevation curves with peaks and troughs in all four transects confirmed the complexity of surface elevation across the intertidal zone (i.e., microtopography). In general, mangrove forests were generally located within the intertidal zone with relative elevation above MSL. Three mangrove species were almost limited within 1-km distance from the shoreline in transects A, B, and C where had positive relative elevations (Fig. 4a-c); however, they were distributed over the 2-km distance in transect D with positive relative elevations (Fig. 4d).

3.2. Link of inundation to mangrove species distribution

To further examine the distribution of different mangrove species along the gradients of elevation and inundation, we conducted spatially explicit quantitative analyses by extracting all grid cells of each species from the land cover classification map and corresponding relative elevation and inundation period. The frequencies of relative elevation for each of the three mangrove species had approximate normal distributions with longer tails at seaward side (Fig. 5). The mean relative elevation for *A. coniculatum* (0.56 m) was lower (statistically significant at $p < 0.05$) than *K. obovate* and *A. marina* which had approximate equal mean relative elevation (0.64 and 0.62 m, respectively). Although these mangrove forests were distributed across a wide elevation range from −0.5 m to 1.5 m, most of them (> 90%) were located within the intertidal zone with relative elevation between MSL and HHW (1.0 m). In fact, the curves of cumulative frequencies indicated that > 90% of grid cells were distributed below HHW for each species.

The areal proportion among three mangrove species changed across the gradient of inundation period (Fig. 6a). *K. obovate* had larger areal proportion (~50%) than the other two species especially at shorter inundation periods, although the areal proportion slightly decreased with increasing inundation. The areal proportion of *A. marina* decreased from ~30% at shorter inundation to ~15% at longer inundation, while the areal proportion of *A. coniculatum* increased significantly from ~10% to ~40% with increasing inundation. Similar spatial patterns were identified when we grouped the inundation gradient into the defined inundation areas including FEA, PEA, AMA, and BMA (Fig. 6b). When the data were arranged as the change in areal proportion of one species itself along the gradient, we found the inundation periods also had approximate normal distributions with longer tails at seaward side (Fig. 6c). Most mangrove forests experienced inundation periods of 1 ~ 8 h/day with differential frequency distribution of inundation periods among species. *K. obovate* was most distributed within an inundation period of 2 ~ 3 h/day, while *A. marina* and *A. coniculatum* were most distributed within a slightly longer inundation period of 3 ~ 4 h/day. Statistical analyses indicated that the change in areal proportion (y) of one species itself along the gradient of inundation period (x) was well described by the following curve: $y = 0.70/(x^2 - 7.28x + 15.85)$ ($R^2 = 0.90$) for *K. obovate*, $y = 0.52/(x^2 - 7.83x + 16.94)$ ($R^2 = 0.96$) for *A. marina*, and $y = 0.66/(x^2 - 8.16x + 20.68)$ ($R^2 = 0.95$) for *A. coniculatum*. By grouping the inundation gradients into the defined inundation areas, > 90% of mangrove forests were situated within AMA and PEA, i.e. < 10% of mangrove forests were situated either above HHW or below MSL (Fig. 6d).

3.3. Influences of inundation on mangrove canopy height

The LiDAR-derived CHM data was combined with the distributions of inundation period to examine the influences of inundation on

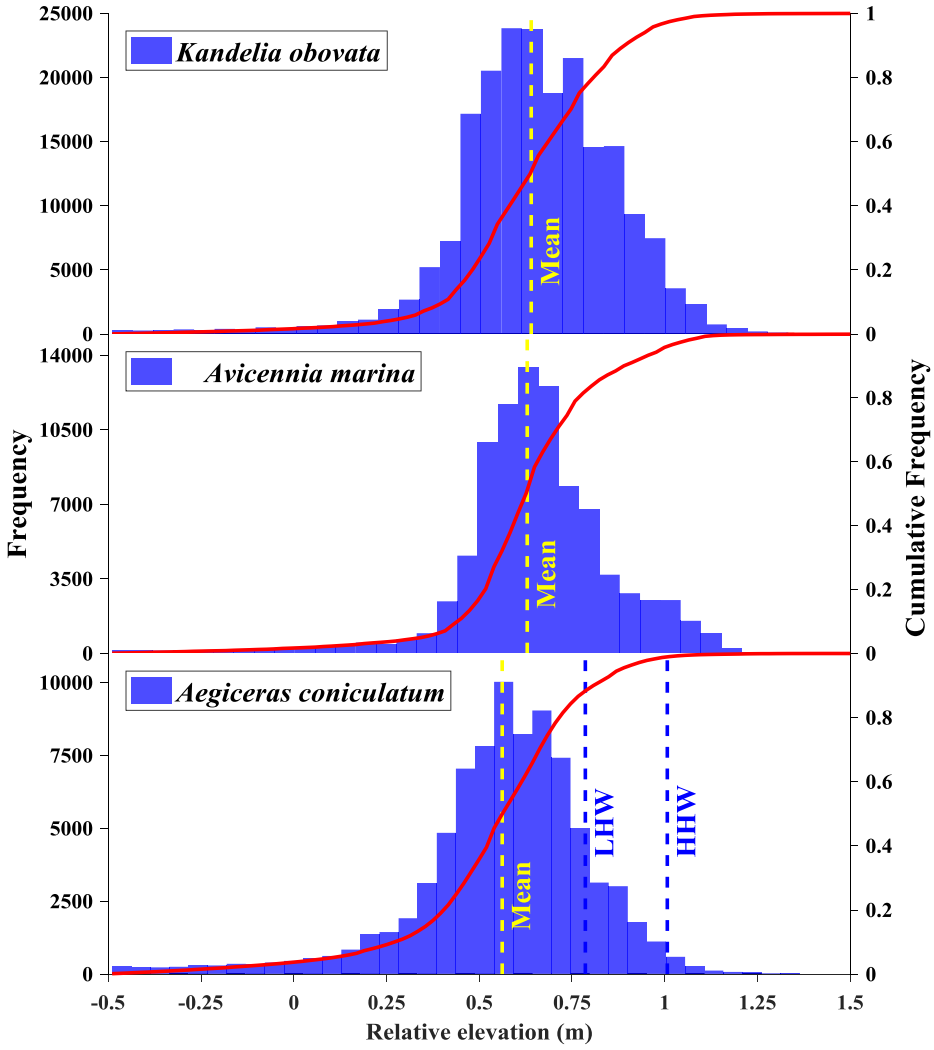

Fig. 5. Frequency distribution (shaded area) and cumulative frequencies (solid lines) of relative elevation for each of three main mangrove species over Zhangjiang estuarine wetland. Mean relative elevation for each species, lower high water (LHW), and higher high water (HHW) were indicated by vertical dashed lines.

mangrove canopy height (Fig. 7). For each mangrove species, all grid cells of canopy height (Fig. 2b) were spatially grouped by inundation period (Fig. 3c) and those grid cells within the upper quantile of each group were used here for analyses. Mangrove forests had different canopy heights among species: *K. obovate* had taller forest canopies with larger height variation (3.8 ~ 6.9 m), while *A. marina* and *A. coniculatum* had shorter forest canopies with smaller height variations (3.3 ~ 5.5 m and 2.3 ~ 3.8 m for each species, respectively). In terms of inundation-height relationships, there were different spatial patterns among species along the inundation gradient. For *K. obovate*, the canopy heights had a hump-shape changing pattern when inundation period was < 4 h/day, while the canopy heights peaked (5.2 ~ 6.9 m) at inundation periods of 4 ~ 6 h/day and gradually decreased with increasing inundation period (Fig. 7a). For both *A. marina* and *A. coniculatum*, the canopy heights had hump-shape changing patterns across the whole inundation gradient with peak heights centered at shorter inundation periods (1 ~ 2 and 2 ~ 3 h/day for each species, respectively; Fig. 7b, c). The quantitative relationships between median values of canopy heights (y) and inundation period (x) were well described by the following curves: $y = (3.76x^2 - 19.35x + 36.01)/(x^2 - 4.82x + 7.98)(R^2 = 0.92)$ for *A. marina* and $y = (1.93x^2 - 3.22x + 9.69)/(x^2 - 1.72x + 6.41)$ ($R^2 = 0.99$) for *A. coniculatum*. It was also noted that the canopy heights of *A. marina* had a steeper declining slope than the other two species. The two-sample Kolmogorov-Smirnov tests were performed to evaluate the differences in canopy heights of adjacent two groups within each species, and the test results indicated that all of canopy heights between adjacent two groups are statistically different at the 5% significance level except the last three groups of *A. marina* and *A. coniculatum* (possibly due to too few pixels for these groups; Fig. 5).

4. Discussion

Our results confirm that the inundation regime plays a critical role in governing the spatial distributions of mangrove species. In accord with general understanding of elevation distributions for mangrove forests (Macnae 1967; Lear and Turner 1977; Alongi 2009), almost all mangrove forests in Zhangjiang estuarine wetland were distributed over the intertidal zone with relative elevation between MSL and HHW (Fig. 5). As a consequence, mangrove forests were on average inundated for < 12 h/day (or < 50% of the time), which was consistent with many other studies (Lewis and Estevez 1988; Iii 2005; Spier et al. 2016). This pattern is expected given that moderate inundation from tidal activities favors mangrove growth (Wang and Zhang 2001; Chen et al. 2004) and intensive inundation suppresses mangrove growth since primary physiological functions of root systems are severely restricted under anaerobic conditions (Pezeshki et al. 1990; Hovenden et al. 1995). In particular, the hump-shape curves of mangrove species distribution along the inundation gradient (Fig. 6c) were consistent with the laboratory experiments of Chen et al. (2005), showing that

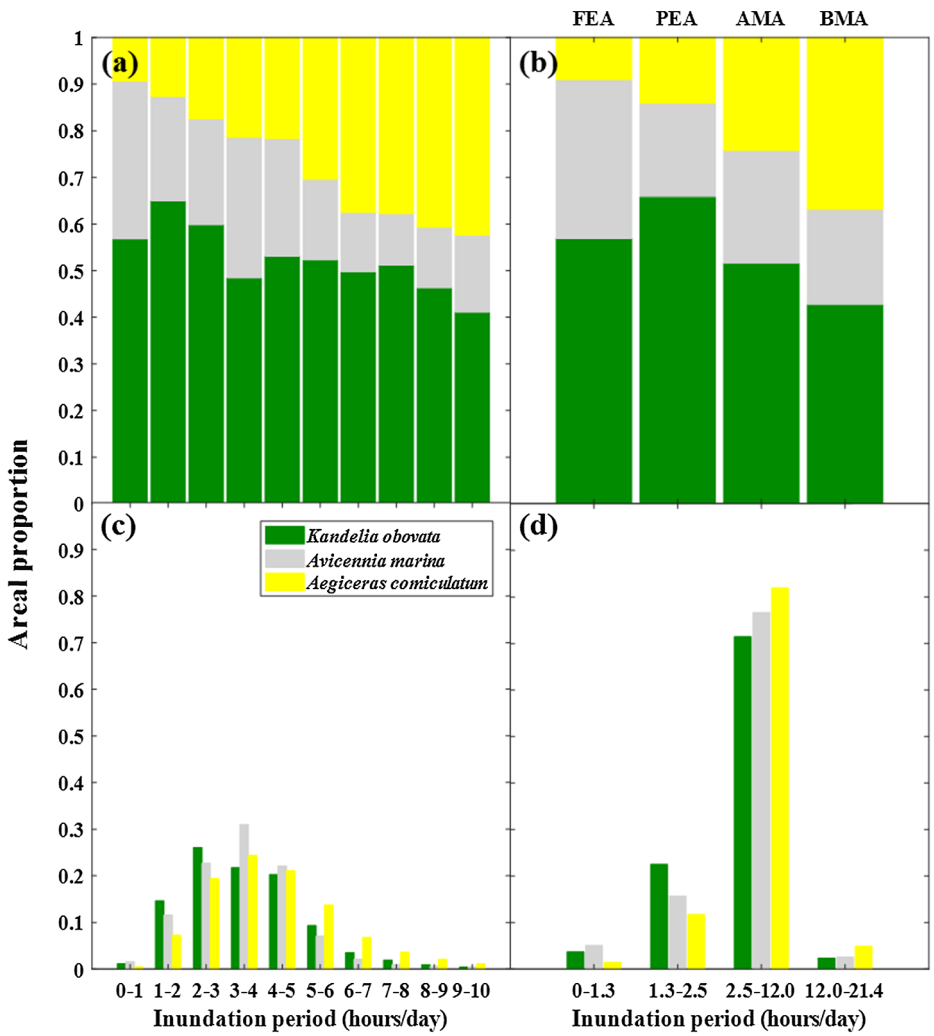

Fig. 6. Changes in spatial distributions of three main mangrove species along with the gradients of inundation period. Each stacked bar in upper panel (a and b) denotes the areal proportion among three species within a gradient, while each series of bar in lower panel (c and d) denotes the change in areal proportion of one species itself along the gradient. The gradients of inundation period are categorized with one-hour interval (left panel) and four varying ranges (right panel) determined from mean tidal regime (see Fig. 3d).

primary physiological activities of mangrove seedlings followed hump-shaped changing patterns with inundation. The favorable inundation periods for mangrove distributions in the field, 2 ~ 5 h/day (Fig. 6c), were comparable with the findings of Chen et al. (2004), who demonstrated that optimal inundation periods for mangrove seedlings were 4 ~ 8 h/day based on artificial tidal experiments in the laboratory.

The spatial distributions of mangrove species over Zhangjiang estuarine wetland did not conform to the hypothesis that mangrove species exhibit strong zonation (no overlaps between species zones) across the intertidal zone. Instead, our spatially explicit quantitative analyses supported a weak zonation pattern (with overlaps between species zones) along the elevation gradient over this wetland. *A. coniculatum* was situated in a lower mean elevation than *K. obovate* and *A. marina*, although obvious overlaps existed in the elevation distributions of different species (Fig. 5). In terms of areal proportion, *A. coniculatum* was relatively more extensively distributed at lower elevations or longer inundation periods, while the other two species were relatively more extensively distributed at higher elevations or shorter inundation periods (Fig. 6a). This weak zonation is expected since strong zonation without any overlaps between mangrove species zones is rarely found in the field (Whittaker 1967; Bunt 1996; Ellison et al. 2000). This weak zonation might also be attributed to the lack of more diverse mangrove species with certain extents and relatively small elevation gradient of mangrove distribution over this wetland (around one meter as shown in Fig. 5). It is worthy to note that only recently had spatially explicit quantitative analyses been applied to test zonation of mangrove species distribution with the accessibility of emerging remote sensing technologies like UAV LiDAR. Thus, previous mangrove zonation studies in the field using transect-based surveys need reexaminations in order to attain more comprehensive assessments.

The hump-shaped changing patterns of mangrove canopy heights along the inundation reflected general understanding on how inundation regime affected mangrove growth over the intertidal zone. Although both mangrove canopy heights and species distributions shared similar changing patterns along the inundation gradient, the optimal inundation periods for the tallest canopies of a given species were inconsistent with those for most distributed zone. For example, the inundation periods for the tallest canopies of *A. marina* and *A. coniculatum* (1 ~ 2 and 2 ~ 3 h/day, respectively; Fig. 7b, c) were shorter than those for most distributed zone (3 ~ 4 h/day; Fig. 6c). This inconsistency could result from differential controlling factors for mangrove species distribution and canopy growth. For example, the dispersal of mangrove embryos and the recruitments of mangrove seedlings may be mainly affected by tidal activities; however, the development of mangrove canopies could be controlled by multiple

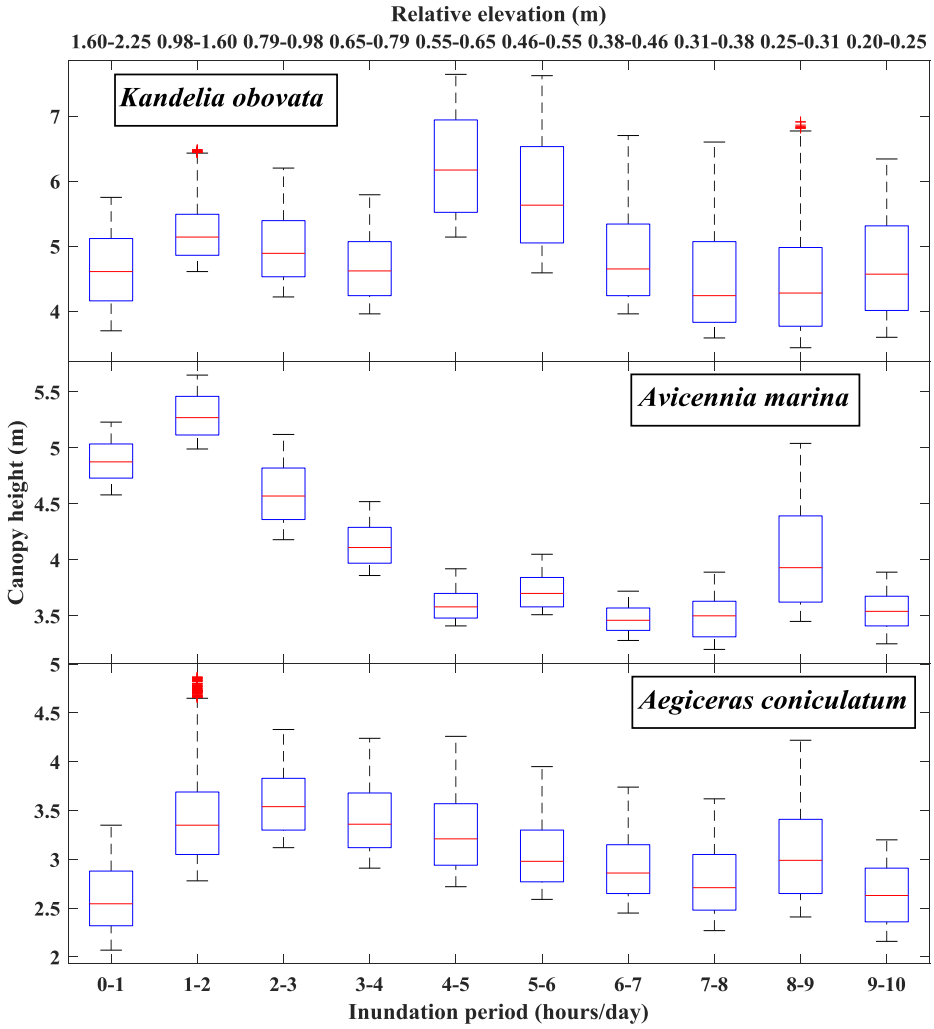

Fig. 7. The changes in canopy heights of three main mangrove species along the gradients of inundation period (lower x-axis) and corresponding relative elevation (upper x-axis).

factors in addition to tidal activities, including nutrient availability, edaphic, and light conditions (Alongi 2009). In fact, mangrove forests over Zhangjiang estuarine wetland were just located to the east of a populated village with intensive aquaculture activities (mainly shrimp ponds), and mangrove canopies landward (closer to the village) tended to grow taller due to more nutrient inputs from water drainage of shrimp ponds. Our results provide evidence that mangrove forests had different inundation sensitivities among species. Taking *A. marina* as an example, narrower elevation distribution (or smaller standard deviation; Fig. 5) and faster decline in areal proportion (Fig. 6a) and canopy height (Fig. 7) along the inundation gradient suggest that *A. marina* was more sensitive to inundation stress compared to the other two species.

This study confirms the practicability of airborne LiDAR in characterizing mangrove canopy heights and underlying microtopography. Compared to most of previous studies, we used a much higher LiDAR point cloud density (around a hundred vs. a few points per meter square), which was proven necessary for accurate retrieving of underlying microtopography under dense mangrove forests as in our study area. The characteristics of low cost, easy control, and feasible flight timing of UAV made it an ideal airborne platform for monitoring periodically inundated mangrove forests that were usually banded or patched distributed in inaccessible estuarine and coastal areas (Giri et al. 2010; Gonçalves and Henriques 2015). Thus, the application of UAV LiDAR technology in this study provided a fresh insight into spatially explicit quantitative analysis of the spatial patterns of mangrove and inundation.

Our spatially explicit quantitative analysis suffered from several major uncertainties. First, the classification errors in mapping mangrove species from RGB image resulted in uncertainty in the spatial distribution of mangrove species. On the one hand, even if we combined LiDAR-derived CHM data and selected the “best” RGB image with the most obvious difference in color among mangrove species over the year, simple RGB spectral information might not be sufficient for image classification. The acquisitions of multi-spectral or hyperspectral images might relieve this issue (Conchedda et al. 2008; Chen et al. 2017; Cao et al. 2018). On the other hand, dense mangrove forests in the study area had overlapped canopies of different species (i.e., mixed pixel issue), which made it challenging to do the mapping. Second, the underlying elevation just below canopy top might not reflect actual elevation of stem bases since lateral growth of tree crowns towards spaces with higher light availability often occurred within mangrove canopies (Grueters et al. 2014). This crown asymmetry issue might have led to the spatial mismatch or offset between mangrove species and inundation periods. Further assessment is needed to determine an optimal spatial resolution to minimize the potential errors from mixed pixel and crown asymmetry. Third, the gap-filling procedure applied to incomplete tidal water level measurements might also have caused error in estimated mean annually inundation period at tidal gauge and thereafter for all grid cells. Further optimization of tidal gauge deployment should be considered to acquire longer time series of

complete tidal water level measurements.

In addition to these uncertainties mentioned above, the errors of spatial mismatching from image-to-image registration between UAV orthomosaic RGB image and LiDAR data products (spatial resolution of 1 m) might affect our quantitative analysis. To explore potential effect from this uncertainty, additional data analysis using resampled spatial imagery at two coarser spatial resolutions (5 m and 10 m) was conducted to see if the identified mangrove-inundation patterns changed with spatial resolution. The results from the additional analysis at coarser spatial resolutions showed approximately the same mangrove-inundation patterns as those at the original spatial resolution (including mangrove species and canopy height distributions with increasing inundation; Fig. S1-3), which further confirmed our findings on the influences of inundation on mangrove growth.

5. Conclusions

Spatially explicit quantitative analyses were conducted in this study to examine the mangrove-inundation spatial patterns, including the influences of inundation on spatial distribution and canopy height of different mangrove species, over the intertidal zone in a subtropical wetland, i.e., Zhangjiang estuarine wetland, Fujian, China. The mapping involved in our analyses, including mangrove species (*K. obovate*, *A. marina* and *A. coniculatum*), canopy height, inundation period, and relative elevation, used multiple remotely sensed data sources, including UAV camera imagery and LiDAR data, and single-point time series measurements of tidal water level. The main findings are summarized as follow. (1) The relative elevations of each mangrove species were in normal distribution over the intertidal zone, and > 90% of mangrove forests were situated within a one-meter elevation gradient between mean sea level and higher high water. (2) The distribution of mangrove species showed similar hump-shaped changing patterns along the inundation gradient but with different optimal inundation periods. (3) Among the three main species, *K. obovate* was distributed more even across the inundation or elevation gradient, and *A. coniculatum* was situated at lower elevations with longer inundation periods. (4) A weak zonation pattern was observed with overlaps between species zones along the elevation gradient over this wetland. (5) The optimal inundation periods for the tallest canopies of a given species were generally shorter than those for most distributed zone, i.e., mangrove canopies in landward side tended to grow taller probably due to higher nutrient inputs. (6) Mangrove forests had differential inundation sensitivities among species with *A. marina* being most sensitive to the inundation stress in this wetland.

We think that this is the first spatially explicit quantitative study to examine the influences of inundation regime on both spatial distribution and canopy height of different mangrove species over the intertidal zone at the landscape scale. This study highlighted the practicability and necessity of the application of high density UAV LiDAR point cloud data in retrieving accurate surface elevation and inundation period at the landscape scale over the intertidal zone of mangrove wetlands. The analysis of mangrove-inundation spatial relationship confirmed the importance of inundation regime as a key driver in regulating the spatial patterns of mangrove forests, which fostered understanding of mangrove-inundation relationship. The determination of appropriate elevation ranges or inundation periods for each mangrove species provided critical knowledge to guide mangrove restoration practices and to assess the vulnerability of mangrove forests in response to future sea level rise.

Acknowledgements

We thank B. Huang and Y. Zhang for their suggestions on designing this study, and thank L. Meng, P. Lin, K. Chen, and C. Zheng for their help in the field work. We also would like to thank the Zhangjiang Estuary Mangrove National Nature Reserve for their long-term support of our ecological research programs. This study was supported by the National Natural Science Foundation of China (31600368), the Natural Science Foundation of Fujian Province, China (2017J01069), the Fundamental Research Funds for the Central Universities of China (20720180118), the Key Laboratory of the Coastal and Wetland Ecosystems, Ministry of Education, China, (WELRI201601) and the State Key Laboratory of Marine Environmental Science, Ministry of Science and Technology, China (MELRI1603).

Appendix A. Supplementary material

Supplementary data to this article can be found online at https://doi.org/10.1016/j.isprsjprs.2019.01.021.

References

Alongi, D.M., 2014. Carbon cycling and storage in mangrove forests. Annual Rev. Marine Sci. 6, 195–219.
Alongi, D.M., 2009. The Energetics of Mangrove Forests. Springer Science & Business Media.
Axelsson, P. (2000). DEM generation from laser scanner data using adaptive TIN models In: International Archives of photogrammetry and remote sensing, Istanbul, Turkey, Vol. XXXIII. Part B4/1, 110-117.
Bunt, J.S., 1996. Mangrove zonation: an examination of data from seventeen riverine estuaries in tropical Australia. Annals Botany 78, 333–341.
Cao, J., Leng, W., Liu, K., Liu, L., He, Z., Zhu, Y., 2018. Object-based mangrove species classification using unmanned aerial vehicle hyperspectral images and digital surface models. Remote Sensing 10.
Chapman, V.J., 1976. Mangrove vegetation. J Cramer 448.
Chen, B., Xiao, X., Li, X., Pan, L., Doughty, R., Ma, J., Dong, J., Qin, Y., Zhao, B., Zhixiang, W., Sun, R., Lan, G., Xie, G., Clinton, N., Chandra, G., 2017. A mangrove forest map of China in 2015: analysis of time series landsat 7/8 and sentinel-1A imagery in Google earth engine cloud computing platform. ISPRS J. Photogrammetry Remote Sens. 131, 104–120.
Chen, L., Wang, W., 2016. Ecophysiological responses of viviparous mangrove *rhizophora stylosa* seedlings to simulated sea-level rise. J. Coastal Res. 336.
Chen, L., Wang, W., Peng, L., 2005. Photosynthetic and physiological responses of *Kandelia candel* L. Druce seedlings to duration of tidal immersion in artificial seawater. Environ. Exp. Bot. 54, 256–266.
Chen, L.Z., Tam, N.F.Y., Wang, W.Q., Zhang, Y.H., Lin, G.H., 2013. Significant niche overlap between native and exotic *Sonneratia* mangrove species along a continuum of varying inundation periods. Estuar. Coast. Shelf Sci. 117, 22–28.
Chen, L.Z., Wang, W.Q., Lin, P., 2004. Influence of water logging time on the growth of *Kandelia candel* seedlings. Acta Oceanologica Sinica 23, 149–157.
Conchedda, G., Durieux, L., Mayaux, P., 2008. An object-based method for mapping and change analysis in mangrove ecosystems. ISPRS J. Photogramm. Remote Sens. 63, 578–589.
Cornforth, W.A., Fatoyinbo, T.E., Freemantle, T.P., Pettorelli, N., 2013. Advanced land observing satellite phased array type L-band SAR (ALOS PALSAR) to inform the conservation of mangroves: Sundarbans as a case study. Remote Sensing 5, 224–237.
Costanza, R., d'Arge, R., de Groot, R., Farber, S., Grasso, M., Hannon, B., Limburg, K., Naeem, S., O'Neill, R.V., Paruelo, J., Raskin, R.G., Sutton, P., van den Belt, M., 1997. The value of the world's ecosystem services and natural capital. Nature 387, 253.
Crase, B., Liedloff, A., Vesk, P.A., Burgman, M.A., Wintle, B.A., 2013. Hydroperiod is the main driver of the spatial pattern of dominance in mangrove communities. Glob. Ecol. Biogeogr. 22, 806–817.
Donato, D.C., Kauffman, J.B., Murdiyarso, D., Kurnianto, S., Stidham, M., Kanninen, M., 2011. Mangroves among the most carbon-rich forests in the tropics. Nat. Geosci. 4, 293–297.
Duncanson, L.I., Dubayah, R.O., Cook, B.D., Rosette, J., Parker, G., 2015. The importance of spatial detail: Assessing the utility of individual crown information and scaling approaches for lidar-based biomass density estimation. Remote Sens. Environ. 168, 102–112.
Ellison, A.M., Mukherjee, B.B., Karim, A., 2000. Testing patterns of zonation in mangroves: scale dependence and environmental correlates in the Sundarbans of Bangladesh. J. Ecol. 88, 813–824.
Fatoyinbo, T., Simard, M., 2013. Height and biomass of mangroves in Africa from ICESat/GLAS and SRTM. Int. J. Remote Sens. 34, 668–681.
Fatoyinbo, T.L., Feliciano, E.A., Lagomasino, D., Lee, S.K., Trettin, C., 2017. Estimating mangrove aboveground biomass from airborne LiDAR data: a case study from the Zambezi River delta. Environ. Res. Lett.
Feliciano, E.A., Wdowinski, S., Potts, M.D., Lee, S.K., Fatoyinbo, T.E., 2017. Estimating mangrove canopy height and above-ground biomass in the everglades national park with airborne LiDAR and TanDEM-X data. Remote Sens. 9.
Giri, C., Ochieng, E., Tieszen, L.L., Zhu, Z., Singh, A., Loveland, T., Masek, J., Duke, N., 2010. Status and distribution of mangrove forests of the world using earth observation satellite data. Glob. Ecol. Biogeogr. 20, 154–159.
Gonçalves, J., Henriques, R., 2015. UAV photogrammetry for topographic monitoring of coastal areas. ISPRS J. Photogramm. Remote Sens. 104, 101–111.
Grueters, U., Seltmann, T., Schmidt, H., Horn, H., Pranchai, A., Vovides, A.G., Peters, R., Vogt, J., Dahdouh-Guebas, F., Berger, U., 2014. The mangrove forest dynamics model

mesoFON. Ecol. Model. 291, 28–41.
Hovenden, M.J., Curran, M., Cole, M.A., Goulter, P.F.E., Skelton, N.J., Allaway, W.G., 1995. Ventilation and respiration in roots of one-year-old seedlings of grey mangrove *Avicennia marina* (Forsk.) Vierh. Hydrobiologia 295, 23–29.
Iii, R.R.L., 2005. Ecological engineering for successful management and restoration of mangrove forests. Ecol. Eng. 24, 403–418.
Kodikara, K.A.S., Mukherjee, N., Jayatissa, L.P., Dahdouh-Guebas, F., Koedam, N., 2017. Have mangrove restoration projects worked? an in-depth study in Sri Lanka. Restoration Ecology 25.
Kovacs, J.M., Lu, X.X., Flores-Verdugo, F., Zhang, C., de Santiago, F.F., Jiao, X., 2013. Applications of ALOS PALSAR for monitoring biophysical parameters of a degraded black mangrove (*Avicennia germinans*) forest. ISPRS J. Photogramm. Remote Sens. 82, 102–111.
Krauss, K.W., Doyle, T.W., Twilley, R.R., Rivera-Monroy, V.H., Sullivan, J.K., 2006. Evaluating the relative contributions of hydroperiod and soil fertility on growth of south Florida mangroves. Hydrobiologia 569, 311–324.
Krauss, K.W., Lovelock, C.E., Mckee, K.L., López-Hoffman, L., Ewe, S.M.L., Sousa, W.P., 2008. Environmental drivers in mangrove establishment and early development: a review. Aquat. Bot. 89, 105–127.
Lagomasino, D., Fatoyinbo, T., Lee, S., Feliciano, E., Trettin, C., Simard, M., 2016. A comparison of mangrove canopy height using multiple independent measurements from land, air, and space. Remote Sensing 8, 327.
Lear, R., Turner, T., 1977. Mangroves of Australia. University of Queensland Press, St. Lucia.
Lee, S.K., Fatoyinbo, T.E., 2017. TanDEM-X Pol-InSAR inversion for mangrove canopy height estimation. IEEE J. Sel. Top. Appl. Earth Obs. Remote Sens. 8, 3608–3618.
Leong, R.C., Friess, D.A., Crase, B., Lee, W.K., Webb, E.L., 2018. High-resolution pattern of mangrove species distribution is controlled by surface elevation. Estuar. Coast. Shelf Sci. 202, 185–192.
Lewis, R.R., Estevez, E.D., 1988. The ecology of Tampa Bay, Florida: an estuarine profile. Biological Report.
Lin, P., 2001. The comprehensive report of science investigation on the natural reserve of mangrove wetland of Zhangjiang Estuary in Fujian. Xiamen University Press, Xiamen, China.
Liu, X.H., Skidmore, A.K., Oosten, H.V., 2002. Integration of classification methods for improvement of land-cover map accuracy. ISPRS J. Photogramm. Remote Sens. 56 (4), 257–268.
Lovelock, C.E., Cahoon, D.R., Friess, D.A., Guntenspergen, G.R., Krauss, K.W., Reef, R., Rogers, K., Saunders, M.L., Sidik, F., Swales, A., 2015. The vulnerability of Indo-Pacific mangrove forests to sea-level rise. Nature 526, 559–563.
Lucas, R., Lule, A.V., Rodríguez, M.T., Kamal, M., Thomas, N., Asbridge, E., Kuenzer, C., 2017. Spatial Ecology of Mangrove Forests: A Remote Sensing Perspective. Mangrove Ecosystems: A Global Biogeographic Perspective. Springer, Cham.
Lucas, R.M., Ellison, J.C., Mitchell, A., Donnelly, B., Finlayson, M., Milne, A.K., 2002. Use of stereo aerial photography for quantifying changes in the extent and height of mangroves in tropical Australia. Wetlands Ecol. Manage. 10, 159–173.
Macnae, W., 1967. Zonation within mangroves associated with estuaries in North Queensland. American Association for the Advancement of Science Publication.
Morris, J.T., Porter, D., Neet, M., Noble, P.A., Schmidt, L., Lapine, L.A., Jensen, J.R., 2005. Integrating LIDAR elevation data, multi-spectral imagery and neural network modelling for marsh characterization. Int. J. Remote Sens. 26, 5221–5234.
Naidoo, G., 1983. Effects of flooding on leaf water potential and stomatal resistance in *Bruguiera gymnorrhiza* (L.) Lam. New Phytologist 93, 369–376.
Nitto, D.D., Neukermans, G., Koedam, N., Defever, H., 2014. Mangroves facing climate change: landward migration potential in response to projected scenarios of sea level rise. Biogeosciences 11, 155–160.
Oh, R.R.Y., Friess, D.A., Brown, B.M., 2017. The role of surface elevation in the re-habilitation of abandoned aquaculture ponds to mangrove forests, Sulawesi, Indonesia. Ecol. Eng. 100, 325–334.
Pezeshki, S.R., Delaune, R.D., Patrick Jr, W.H., 1990. Differential response of selected mangroves to soil flooding and salinity: gas exchange and biomass partitioning. Can. J. For. Res. 20, 869–874.
Pugh, D.T., Faull, H.E., 1983. Tides, surges and mean sea level trends. Thomas Telford.
Snedaker, S.C., 1982. Mangrove species zonation: why? In Contributions to the Ecology of Halophytes, Springer, Dordrecht.
Soininen, A., 2012. TerraScan User's Guide. Southampton, UK, The National Mapping Agency of Great Britain.
Spier, D., Gerum, H.L.N., Noernberg, M.A., Lana, P.C., 2016. Flood regime as a driver of the distribution of mangrove and salt marsh species in a subtropical estuary. J. Mar. Syst. 161, 11–25.
Valiela, I., Bowen, J.L., York, J.K., 2001. Mangrove forests: One of the world's threatened major tropicalenvironments. Bioscience 51, 807–815.
Wang, W.Q., Zhang, F.S., 2001. The physiological and molecular mechanism of adaptation to anaerobiosis in higher plants. Plant Physiol. Commun. 37, 63–70.
Wannasiri, W., Nagai, M., Honda, K., Santitamnont, P., Miphokasap, P., 2013. Extraction of mangrove biophysical parameters using airborne LiDAR. Remote Sensing 5, 1787–1808.
Watson, J.G., 1928. Mangrove forests of the Malay Peninsula. Malayan Forest Records 6.
Whittaker, R.H., 1967. Gradient analysis of vegetation. Biol. Rev. 42, 207–264.
Zhao, F., Guo, Q., Kelly, M., 2012. Allometric equation choice impacts LiDAR-based forest biomass estimates: A case study from the Sierra National Forest, CA. Agric. For. Meteorol. 165, 64–72.
Zolkos, S.G., Goetz, S.J., Dubayah, R., 2013. A meta-analysis of terrestrial aboveground biomass estimation using lidar remote sensing. Remote Sens. Environ. 128, 289–298.